# Chromophore Structure in Lumirhodopsin and Metarhodopsin I by Time-Resolved Resonance Raman Microchip Spectroscopy†

Duohai Pan and Richard A. Mathies*

*Department of Chemistry, University of California, Berkeley, California 94720*

*Received April 3, 2001; Revised Manuscript Received May 7, 2001*

ABSTRACT: Time-resolved resonance Raman microchip flow experiments have been performed on the lumirhodopsin (Lumi) and metarhodopsin I (Meta I) photointermediates of rhodopsin at room temperature to elucidate the structure of the chromophore in each species as well as changes in protein−chromophore interactions. Transient Raman spectra of Lumi and Meta I with delay times of 16 $\mu$s and 1 ms, respectively, are obtained by using a microprobe system to focus displaced pump and probe laser beams in a microfabricated flow channel and to detect the scattering. The fingerprint modes of both species are very similar and characteristic of an all-trans chromophore. Lumi exhibits a relatively normal hydrogen-out-of-plane (HOOP) doublet at 951/959 $cm^{-1}$, while Meta I has a single HOOP band at 957 $cm^{-1}$. These results suggest that the transitions from bathorhodopsin to Lumi and Meta I involve a relaxation of the chromophore to a more planar all-trans conformation and the elimination of the structural perturbation that uncouples the 11H and 12H wags in bathorhodopsin. Surprisingly, the protonated Schiff base C═N stretching mode in Lumi (1638 $cm^{-1}$) is unusually low compared to those in rhodopsin and bathorhodopsin, and the C═ND stretching mode shifts down by only 7 $cm^{-1}$ in $D_2O$ buffer. This indicates that the Schiff base hydrogen bonding is dramatically weakened in the bathorhodopsin to Lumi transition. However, the C═N stretching mode in Meta I is found at 1654 $cm^{-1}$ and exhibits a normal deuteration-induced downshift of 24 $cm^{-1}$, identical to that of the all-trans protonated Schiff base. The structural relaxation of the chromophore−protein complex in the bathorhodopsin to Lumi transition thus appears to drive the Schiff base group out of its hydrogen-bonded environment near Glu113, and the hydrogen bonding recovers to a normal solvated PSB value but presumably a different hydrogen bond acceptor with the formation of Meta I.

Rhodopsin, the major protein in the disk membranes of retinal rod cells, is a seven-α-helix transmembrane receptor containing an 11-*cis*-retinal prosthetic group bound to Lys296 (*1*). When rhodopsin absorbs a photon, its 11-*cis*-retinal protonated Schiff base (PSB)[1] chromophore rapidly isomerizes to photorhodopsin (*2*) followed by relaxation to bathorhodopsin, both of which contain a distorted all-trans chromophore (*3*). Bathorhodopsin thermally decays through a series of forms called the blue-shifted intermediate (BSI), lumirhodopsin (Lumi), metarhodopsin I (Meta I), and metarhodopsin II (Meta II) as shown in Figure 1 (*4*). The Meta II intermediate catalyzes the activation of the G-protein transducin, which couples the optical excitation signal to an enzymatic cascade and the generation of an optic nerve impulse (*5*).

Spectroscopic work has provided a good understanding of the molecular mechanism of the early events in the visual excitation process. Femtosecond time-resolved absorption experiments revealed that the cis−trans isomerization of the rhodopsin chromophore is complete in only 200 fs (*2*, *6*). The photorhodopsin product, which is thought to contain a hot and/or conformationally distorted form of the trans chromophore (*3*), relaxes to bathorhodopsin in ∼5 ps (*7*). The chromophore structure in bathorhodopsin has been studied in great detail because bathorhodopsin is the first intermediate that can be trapped by cooling to 77 K. Resonance Raman experiments on bathorhodopsin reveal unusually intense hydrogen-out-of-plane (HOOP) wagging vibrations in the 850−920 $cm^{-1}$ region, which indicate that the chromophore is distorted and strongly perturbed near $C_{12}$ (*8*, *9*). Surprisingly, these characteristic vibrations are also observed in the 2 ps time-resolved resonance Raman spectrum of bathorhodopsin at room temperature (*3*). This observation demonstrates that the basic structural features of this high-energy intermediate are the same when it is trapped kinetically or thermally. Systematic resonance Raman studies on rhodopsin and bathorhodopsin based on isotopically labeled derivatives suggest that electronic and conformational distortion is the most likely cause of the significant energy storage in the primary photoproduct (146 kJ/mol) that drives the activating protein conformational changes (*8*, *10*, *11*).

The later intermediates in the rhodopsin bleaching process have also been extensively characterized. BSI is entropically favored and thus is not trapped at low temperatures, but

† This work was supported by a grant from the NIH (EY02051).

* To whom correspondence should be addressed. Phone: (510) 642-4192. Fax: (510) 642-3599. E-mail: rich@zinc.cchem.berkeley.edu.

[1] Abbreviations: PSB, protonated Schiff base; BSI, blue-shifted intermediate; Lumi, lumirhodopsin; Meta I, metarhodopsin I; Meta II, metarhodopsin II; HOOP, hydrogen-out-of-plane; CARS, coherent anti-Stokes Raman spectroscopy; ROS, rod outer segments; PEEK, polyetheretherketone; CCD, charge-coupled device; Batho, bathorhodopsin.

10.1021/bi010670x CCC: $20.00 
Published on Web 06/07/2001

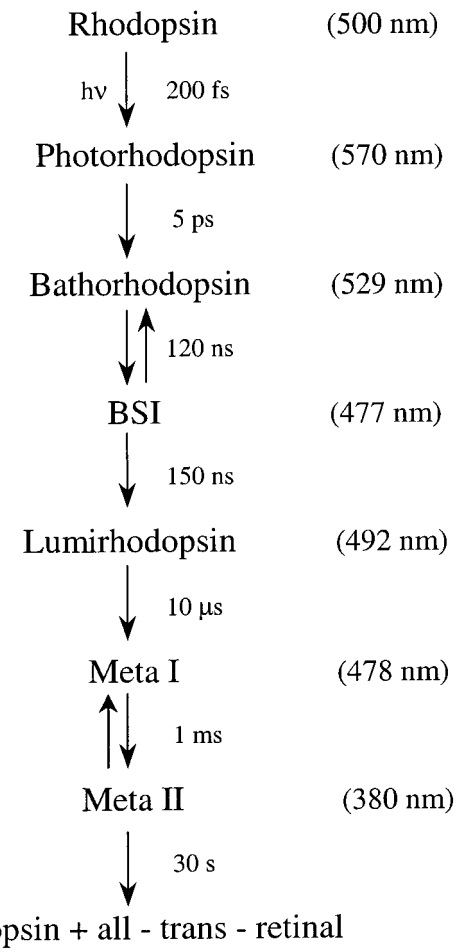


FIGURE 1: Rhodopsin photobleaching sequence.

evidence suggests that the formation of BSI triggers some protein conformational change (*12*, *13*). The decay of the Lumi, Meta I, and Meta II intermediates has been studied with kinetic absorption spectroscopy (*4*, *14*). The rate of the Lumi to Meta I transformation exhibits a strong temperature and pH dependence (*4*). FTIR data (*15*−*17*) together with NMR (*18*, *19*) as well as linear dichroism measurements (*20*) showed that the chromophore in the Lumi and Meta I species has relaxed relative to its more strained all-trans form in bathorhodopsin (*4*).

Thermal trapping methods are limited to studying intermediates with successively higher thermal barriers, and can thus miss transitions dominated by significant entropy changes. It is thus desirable to study the structure of rhodopsin's intermediates under room-temperature conditions that are physiologically relevant. Resonance Raman vibrational spectra of the metarhodopsin intermediates were first obtained by stabilization at either high (Meta I) or low (Meta II) pH (*21*). Time-resolved CARS (coherent anti-Stokes Raman spectroscopy) spectra of Lumi at room temperature have also been reported (*22*). However, the characterization of the linkage between the chromophore and the protein in the Lumi and Meta I species was not revealed in these CARS studies, and complete high-quality vibrational spectra of Lumi and Meta I are not yet available. The development of convenient methods for routinely obtaining time-resolved resonance Raman spectra of intermediates on the millisecond to microsecond time scale would facilitate vibrational structural studies of BSI, Lumi, and Meta I.

We present here a new Raman microchip flow technique that permits the facile study of rhodopsin's microsecond to millisecond photointermediates. It is based on the combination of our Raman microprobe system with rapid-flow techniques. The Raman microprobe system was first developed in 1982 (*23*) and was used to obtain Raman spectra of single visual pigment cells as well as in vitro samples of expressed pigments (*24*−*28*). Rapid-flow methods (*29*) have been used to obtain time-resolved spectra of photolytic intermediates for many years using multiple-beam techniques (*30*). A drawback of these flow approaches is the large amount of pigment needed when working at a high flow rate. A solution to this problem is suggested by the recent development of microfabricated lab-on-a-chip systems (*31*) that permit the production of precisely tailored and complex layouts of microchannels (*32*, *33*). We were thereby encouraged to make microchannel flow systems for time-resolved resonance Raman studies where the cross section of the flow channel is made very small and matched to the confocal profile of the laser beam in the micro-probe system.

We have used the Raman microchip flow method to obtain high-quality transient Raman spectra of the Lumi and Meta I species at room temperature. Two displaced laser beams initiate the rhodopsin photochemistry and measure the Raman spectrum of the intermediate. The flow rates and spatial separation between the pump and probe beams are chosen to give the desired time delay ranging from several hundred nanoseconds to several milliseconds. High-quality Raman spectra of Lumi and Meta I are obtained that allow us to clarify vibrational mode assignments. Furthermore, the Raman spectra of Lumi and Meta I in $D_2O$ buffer are used to elucidate how the hydrogen bonding of the Schiff base changes as the activating protein conformational changes occur. The structure of the chromophore in the Lumi and Meta I intermediates and their structural changes are discussed on the basis of these data.

## MATERIALS AND METHODS

*Preparation of Rhodopsin*. Rhodopsin was isolated from 100 bovine retinas (J. A. Lawson, Lincoln, NE) by sucrose flotation followed by sucrose density gradient centrifugation as described previously (*8*). The yield was typically 12−15 nmol of rhodopsin per retina. The isolated rod outer segments (ROS) were lysed in water and solubilized in 15 mL of 5% Ammonyx-LO (Exciton, Dayton, OH). The resulting rhodopsin solution was further purified with a hydroxylapatite column (*34*). The final samples [150 mM phosphate buffer (pH 7) and 7−11 mM $NH_2OH$] had an absorbance of 2.0−2.5 OD/cm at 500 nm, and 280 nm/500 nm ratios were 1.76−1.90.

*Time-Resolved Resonance Raman Spectroscopy*. Transient Raman spectra were obtained using a two-beam, pump−probe configuration employing a Raman microprobe for detection and a microchip flow system (see Figure 2). A detailed description of the Raman microprobe apparatus and two-beam system for low-temperature, steady-state experiments was reported previously (*25*). Briefly, a beam splitter (50/50) was first used to make the probe and pump beams near collinear. The pump and probe beams were then focused with a 250 mm cylindrical lens at the microscope focal plane. The line image of the beam was subsequently focused on

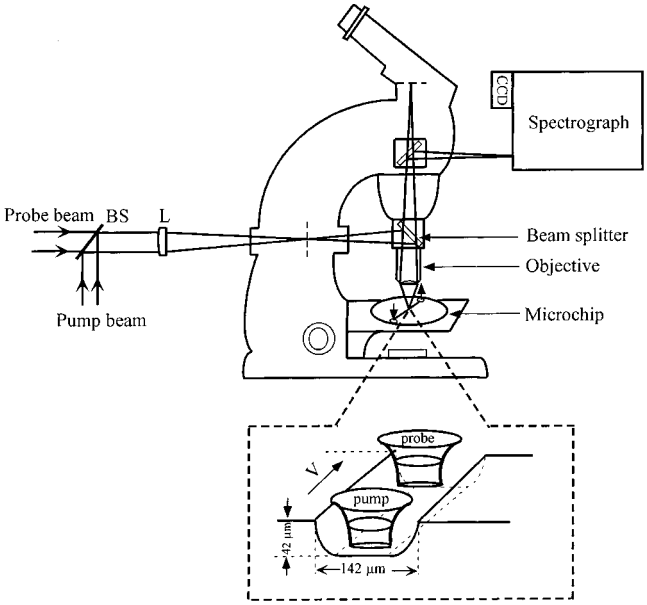


FIGURE 2: Time-resolved resonance Raman microchip apparatus. The two cylindrically focused beams are displaced along the flow direction. The beam separation and flow velocity determine the time delay. The pump beam was focused to a 5−10 $\mu$m × 100 $\mu$m spot, and the probe beam was 5 $\mu$m × 100 $\mu$m. The expanded chip view shows just the bottom etched wafer that makes up the bonded two-layer glass sandwich.

the sample by a 40× NA 0.6 objective lens to form an ∼5 $\mu$m × 100 $\mu$m spot for the probe and an ∼5−10 $\mu$m × 100 $\mu$m spot for the pump. Backscattered Raman light was collected by the same objective and focused at the entrance slit of the subtractive dispersion, double spectrograph (*35*). An aperture was used to limit the slit height so that scattering originating from the channel walls was blocked. The spatial separation between the two beams was controlled by adjusting the beam splitter position with a translation stage. The beam image size and its alignment with respect to the entrance slit of the spectrometer were determined by viewing the fluorescence from a slide coated with rhodamine-6G. The sample was pumped once through the chip microchannel by applying nitrogen gas pressure to the sample reservoir (20−130 psi). The sample reservoir was cooled with ice to 4 °C.

The microchips were fabricated on glass substrates using photolithography, wet chemical etching, and thermal bonding methods (*31*). A glass wafer was coated with photoresist and then exposed through a Cr mask to define the channel pattern. After development of the photoresist, the channel pattern was etched in the substrate with hydrofluoric acid. The remaining photoresist was removed; the etched wafer reservoirs were drilled at either end of the channel, and then the double-layer sandwich was formed by thermal bonding to a second wafer. PEEK (polyetheretherketone) polymer flexible tubing (256 $\mu$m inside diameter, 1.0 mm outside diameter) is fitted into the drilled holes and sealed with epoxy to introduce solution into the micro-flow cell. The advantage of this microfabricated system is that very small amounts of sample are needed because the flow cross section can be made very close to the imaged laser beam size. The channel dimensions of the chip used in our experiments are ∼42 $\mu$m deep × 142 $\mu$m wide. Thus, for the Lumi and Meta I experiments reported here, only 4 and 1 mL of sample were required, respectively, for the pump-plus-probe spectra and only 1 mL was needed for the probe-only spectra.

The laser powers and flow rates were chosen to give the desired time delays and photoalteration parameters *F* (*29*). The transient Raman spectrum of Lumi was obtained using a 514.5 nm probe beam (500 $\mu$W) and a near collinear 488 nm pump beam (2.5 mW), with photoalteration parameters of 0.3 and 2.5−3, respectively. The Meta I spectrum was obtained with a 476.5 nm probe beam (300 $\mu$W) and a 2 mW, 531 nm pump. Lumi is formed several microseconds after the decay of BSI, and its lifetime is on the order of tens of microseconds (*4*). In our experiment, the Lumi Raman scattering was obtained with a delay time of 16 $\mu$s (spatial separation of 18 $\mu$m and flow rate of 113 cm/s). For the Meta I spectrum, the desired time delay of ∼1 ms was provided by a 12 cm/s flow rate and an ∼120 $\mu$m separation.

The microchip flow system was also found to be advantageous for data collection because it provided more reproducible background subtractions as well as better imaging and collection of the scattered light. The Raman signal was collected from a 5 $\mu$m × 100 $\mu$m area approximately 50 $\mu$m deep. Typically, the optical density of the sample is ∼2.0−2.5 $cm^{-1}$ at 500 nm, giving an OD of ∼0.01 in the channel. It was necessary to record ten ∼1 min exposures for each experimental configuration. Cosmic ray spikes were removed from each spectrum before summation. The subtractive dispersion Spex 1400 double spectrograph was equipped with 500 nm blazed, 600 and 1200 grooves/mm gratings. Raman spectra were detected with a nitrogen-cooled CCD detector (LN/CCD-1152, Princeton Instruments) controlled by an ST-130 controller. The detector consists of a 1152 × 298 pixel array with a 26 mm × 6.7 mm photosensitive area that detected Raman signals over a 1400 $cm^{-1}$ range. The fluorescence background was removed by subtracting a bleached rhodopsin spectrum. The known cyclohexanone Raman bands were used to calibrate the spectra. The sensitivity of the detection system as a function of wavelength was corrected using a white light spectrum. The reported frequencies are accurate within ±2 $cm^{-1}$, and the resolution of the spectra is 6 $cm^{-1}$.

## RESULTS

Figure 3 presents the results of a time-resolved Raman microchip flow experiment with a 16 $\mu$s time delay that was designed to obtain a spectrum of the Lumi intermediate. The pump wavelength is 488 nm, and the probe wavelength is 514.5 nm, which lies on the red side of the Lumi absorption band. The probe-only Raman spectrum presented in Figure 3B is unambiguously dominated by rhodopsin scattering. The most intense peak at 1546 $cm^{-1}$ is due to ethylenic C=C stretching. The fingerprint modes at 1188, 1215, 1237, and 1268 $cm^{-1}$ are assigned to the $C_{14}-C_{15}$, $C_8-C_9$, and $C_{12}-C_{13}$ stretches, and the 11H + 12H rock combination, respectively (*36*). The peaks located between 950 and 1020 $cm^{-1}$ are hydrogen-out-of-plane (HOOP) wagging and $C-CH_3$ rocking modes. The pump-plus-probe spectrum in Figure 3A exhibits new peaks at 951, 1155, and 1205 $cm^{-1}$, indicating that it contains a mixture of scattering from rhodopsin and a new intermediate species. Indicated amounts of the probe-only spectrum were subtracted from the pump-plus-probe spectrum to identify the optimal subtraction

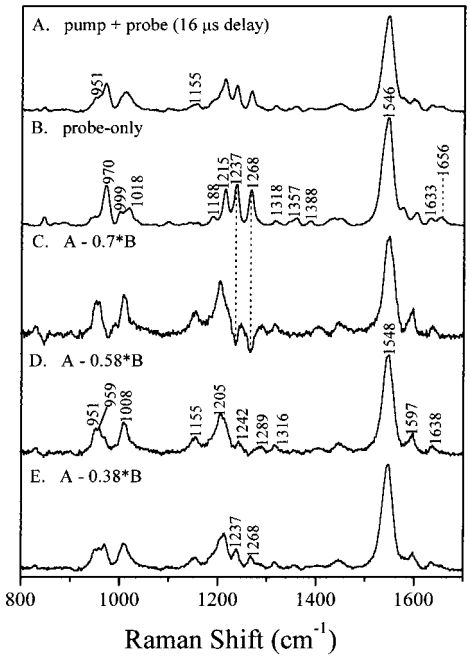


FIGURE 3: Time-resolved (16 $\mu$s delay) resonance Raman microchip spectra of lumirhodopsin: (A) pump-plus-probe spectrum and (B) probe-only spectrum. Spectra C−E are lumirhodopsin spectra obtained by subtracting the indicated fractions of the probe-only spectrum from the pump-plus-probe spectrum. The optimum subtraction coefficient was determined to be 0.58. The pump wavelength was 488 nm, and the probe wavelength was 514.5 nm. A typical Lumi spectrum required only 5 mL of sample.

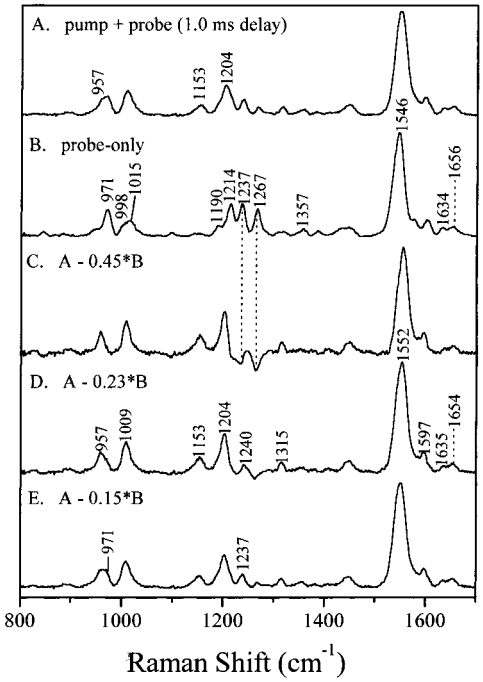


FIGURE 4: Time-resolved (1 ms delay) resonance Raman microchip spectra of metarhodopsin I: (A) pump-plus-probe spectrum and (B) probe-only spectrum. Spectra C−E are metarhodopsin I spectra obtained by subtracting the indicated fractions of the probe-only spectrum from the pump-plus-probe spectrum. The optimum subtraction coefficient was determined to be 0.23. The pump and probe excitation wavelengths were 531 and 476.5 nm, respectively. A typical Meta I spectrum required only 2 mL of sample.

parameter for generating a pure Raman spectrum of Lumi. A subtraction parameter of 0.58 was determined to be optimal (Figure 3D) because it minimizes positive features from the prominent 970, 1237, and 1268 $cm^{-1}$ bands of rhodopsin without introducing spurious derivative band shapes or negative peaks. The calculated photoalteration parameter of the pump beam (3.5) was in qualitative agreement with the subtraction parameter and the fact that ~64% of the sample was bleached.

In the Lumi spectrum, the strong band at 1548 $cm^{-1}$ is assigned to the ethylenic mode. This ethylenic band is consistent with the 492 nm absorption band maximum for Lumi (*4*), based on the correlation of the ethylenic frequencies of retinals with their absorption maxima (*27*). An ethylenic mode at 1548 $cm^{-1}$ was also observed in the Lumi CARS spectrum (*22*). In the fingerprint region, five bands at 1155, 1205, 1214 (sh), 1242, and 1289 $cm^{-1}$ are observed. The vibrational pattern in the fingerprint region of Lumi is similar to that of the all-trans retinal protonated Schiff base (*37*) and bathorhodopsin (*8*). The PSB modes have been assigned with isotopically labeled chromophores and retinal analogues (*8*). On the basis of this comparison, the line at 1155 $cm^{-1}$ in Lumi corresponds to the $C_{10}-C_{11}$ stretch, which is 4 $cm^{-1}$ lower than the corresponding mode of the all-trans retinal PSB, and 11 $cm^{-1}$ below the $C_{10}-C_{11}$ stretch in bathorhodopsin (*8*). The 1205 $cm^{-1}$ line corresponds to the $C_{14}-C_{15}$ stretch and the shoulder at 1214 $cm^{-1}$ to the $C_8-C_9$ stretch, and the 1242 $cm^{-1}$ is assigned to the $C_{12}-C_{13}$ stretch. The 1289 $cm^{-1}$ line is assigned to the 11H + 12H rock combination mode. The frequency shifts between Lumi and the all-trans retinal PSB for the $C_8-C_9$, $C_{10}-C_{11}$, $C_{12}-C_{13}$, and $C_{14}-C_{15}$ stretches are 11, −4, 5, and 13 $cm^{-1}$, respectively. The assignment of the $C_{14}-C_{15}$, $C_8-C_9$, and $C_{12}-C_{13}$ stretching modes to 1205, 1214, and 1238 $cm^{-1}$, respectively, in the FTIR difference spectra of Lumi (*15*) also supports our results.

In the region between 850 and 1020 $cm^{-1}$, the hydrogen-out-of-plane (HOOP) wagging vibrations are expected for the retinal chromophore. For Lumi, only a new doublet at 951/959 $cm^{-1}$ was detected, fairly consistent with the observation of a doublet at 940/947 $cm^{-1}$ in the Lumi FTIR spectrum (*15*). Ohkita and co-workers reported a broad band at ~947 $cm^{-1}$ in the Lumi FTIR spectrum and assigned this band to the 11H and 12H $A_u$ HOOP vibration mode based on specifically deuterated retinal derivatives (*17*). A 944 $cm^{-1}$ band was also found in a recent CARS study of Lumi (*22*). The doublet is close to the frequency of the HOOP mode measured in the all-trans retinal PSB at ~965−980 $cm^{-1}$ (*37*). In addition, the intense line at 1008 $cm^{-1}$ is assigned to a methyl rocking vibrational mode based on its traditional frequency (*38*).

Figure 4 presents results of time-resolved resonance Raman microchip flow experiments with a time delay of ~1 ms to obtain a spectrum of Meta I. First, a probe-only Raman spectrum of rhodopsin was obtained using 476.5 nm excitation (Figure 4B). Adding a 531 nm pump beam (Figure 4A) significantly reduces the intensities of bands due to the rhodopsin species. Subtraction of the probe-only spectrum (×0.23) from the pump-plus-probe spectrum to minimize positive or negative 971, 1237, and 1267 $cm^{-1}$ bands of rhodopsin yields the difference spectrum (Figure 4D). The ~82% experimental sample bleach is consistent with the subtraction parameter of 0.23.

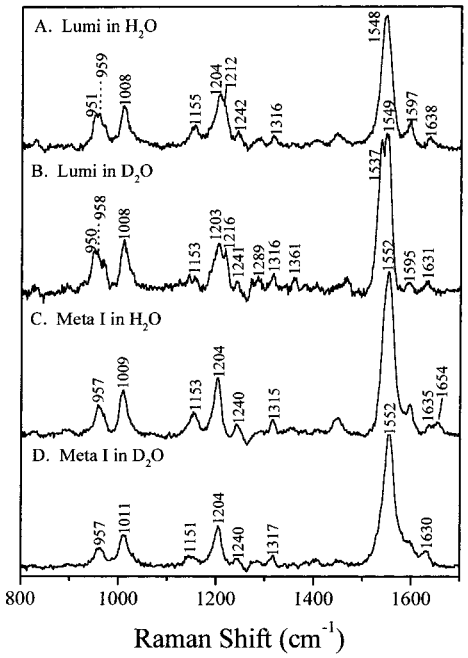


FIGURE 5: Time-resolved resonance Raman microchip spectra of lumirhodopsin in (A) $H_2O$ and (B) $D_2O$ and of metarhodopsin I in (C) $H_2O$ and (D) $D_2O$.

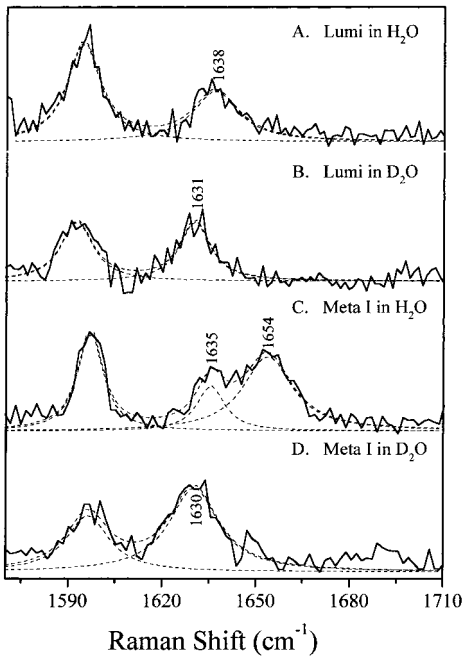


FIGURE 6: Schiff base regions of the Raman spectra of lumirhodopsin in (A) $H_2O$ and (B) $D_2O$ and of metarhodopsin I in (C) $H_2O$ and (D) $D_2O$. Lorentzian fits to the bands are indicated by the dashed lines. The indicated frequencies are those of the band components.

The Meta I spectrum is characterized by its distinctive 1552 $cm^{-1}$ ethylenic mode, which is ~6 $cm^{-1}$ higher than that of rhodopsin, in agreement with the previous Meta I spectra (*21*). The Meta I fingerprint modes are identical to those of Lumi. By analogy to the work of Lumi, the band at 1153 $cm^{-1}$ is assigned to the $C_{10}-C_{11}$ stretch, the band at 1204 $cm^{-1}$ is assigned to the $C_{14}-C_{15}$ stretch, and the shoulder at 1216 $cm^{-1}$ is the $C_8-C_9$ stretch. The 1240 $cm^{-1}$ band is assigned as the $C_{12}-C_{13}$ vibrational stretch. There are minor differences in the fingerprint region between our results and previous data (*21*). Doukas et al. observed that the $C_{10}-C_{11}$ and $C_{14}-C_{15}$ modes were located at 1159 and 1189 $cm^{-1}$, respectively. This discrepancy probably results from the 5% rhodopsin and or isorhodopsin, which coexisted in their experiments (*21*). The major HOOP peak in the Meta I spectrum appears at 957 $cm^{-1}$, corresponding to an in-phase combination mode of the 11H and 12H wags. The 1009 $cm^{-1}$ feature is assigned to the methyl rocking vibration mode, based on correspondence to the all-trans retinal PSB mode at 1012 $cm^{-1}$ (*8*). These assignments are consistent with the earlier Meta I Raman spectrum (*21*) as well as its FTIR spectra (*15*−*17*).

Figure 5 presents time-resolved resonance Raman microchip spectra of Lumi and Meta I in $H_2O$ and $D_2O$. An expanded view of the Schiff base region of the Lumi and Meta I spectra in $H_2O$ and $D_2O$ will be found in Figure 6. The Lumi Raman band at 1638 $cm^{-1}$ shifts down to 1631 $cm^{-1}$ after dialysis in a $D_2O$ buffer (Figure 6A,B). This band is thus due to a protonated Schiff base linkage between the chromophore and the protein which shifts down because the stretching mode is coupled to the N−H rocking vibration. These observations are consistent with the difference FTIR studies in which the C═NH stretch at 1635 $cm^{-1}$ exhibits a deuteration-induced downshift of 4 $cm^{-1}$ (*15*). For Meta I, the protonated Schiff baseline at 1654 $cm^{-1}$ shifts down to 1630 $cm^{-1}$, overlapping the 1635 $cm^{-1}$ mode, after the protein is suspended in $D_2O$ buffer. Meta I FTIR studies at low temperatures (*39*) gave a similar result, and Doukas et al. assigned the 1657 $cm^{-1}$ band in the Meta I Raman spectrum to the C═NH stretch (*21*). The band at 1635 $cm^{-1}$ adjacent to the C═NH band in Figure 6C is assigned to a localized C═C stretching which is analogous to the 1633 $cm^{-1}$ mode observed in the spectra of rhodopsin and isorhodopsin (*8*, *26*). The C═NH and C═ND stretching frequencies of rhodopsin, Lumi, and Meta I are compared with previous data as well as those of bathorhodopsin in Table 1. Note that the Schiff base C═N stretch at 1654 $cm^{-1}$ in the Meta I spectrum is similar to that of rhodopsin and bathorhodopsin. However, the C═N stretching frequency in Lumi is unusually low compared to that of rhodopsin. Also, the $D_2O$-induced shift for Meta I (~24 $cm^{-1}$) is somewhat smaller than that for rhodopsin, while the shift for Lumi is unusually small (~7 $cm^{-1}$).

Table 1: Schiff Base Frequencies for Rhodopsin and Its Photoproducts

| | C═NH | | C═ND | | shift ($cm^{-1}$) | |
|---|---|---|---|---|---|---|
| pigment | RR | IR[c] | RR | IR[c] | RR | IR[c] |
| rhodopsin | 1656 | 1659 | 1625 | 1639 | 31 | 30 |
| Batho | 1654,[a] 1657[b] | 1659 | 1626,[a] 1625[b] | 1639 | 28,[a] 31[b] | 30 |
| Lumi | 1638 | 1635 | 1631 | 1631 | 7 | 4 |
| Meta I | 1654, 1657[d] | 1652 | 1630 | 1630 | 24 | 22 |
| all-trans PSB | 1654[e] | 1656[f] | 1631[e] | 1633[f] | 23[e] | 23[f] |

[a] From ref *8*. [b] From ref *9*. [c] From ref *15*. [d] From ref *21*. [e] From ref *38*. [f] From ref *46*.

## DISCUSSION

The structure of the chromophore in the Lumi and Meta I intermediates in the rhodopsin photoreaction cascade is a key element in understanding how the chromophore interacts with the protein as the activating protein conformational changes occur. The vibrational features in the skeletal

fingerprint region of the Lumi Raman spectrum are nearly identical to those of the all-trans retinal PSB, indicating that the skeletal structure of chromophore in Lumi is all-trans. This is consistent with circular dichroism (CD) measurements, where the strong negative CD signal of bathorhodopsin changes to a weak negative signal in Lumi, indicating a conformational change of the $C_9-C_{13}$ portion toward a relaxed trans structure (*40*). However, the $C_8-C_9$ stretching band in Lumi at 1214 $cm^{-1}$ is 11 $cm^{-1}$ higher than in the all-trans retinal PSB, suggesting that its electronic structure is more delocalized (*8*). Inspection of the fingerprint region of the Meta I spectrum does not reveal any major differences between Lumi and Meta I. The similarity of the fingerprint regions of the Lumi and Meta I species indicates that the transition from Lumi to Meta I does not significantly alter the all-trans chromophore skeletal structure.

The HOOP vibrations of the retinal prosthetic group provide a probe of the conformational distortion of the chromophore. Selective deuteration of the retinal chromophore was used by Eyring et al. to assign the 854, 876, and 921 $cm^{-1}$ modes of bathorhodopsin to the $C_{14}H$, $C_{10}H$, and $C_{11}H$ HOOP wags, respectively (*9*). The $C_{11}H$ and $C_{12}H$ wags are unusually decoupled in bathorhodopsin, which is thought to result from the presence of a strong perturbation near $C_{12}H$. The unusually strong intensities of these modes indicate a twisted high-energy chromophore structure (*9*, *10*). In the Lumi spectrum, a new doublet HOOP band at 951/959 $cm^{-1}$ is observed. Although the definite assignment of this band has not yet been made, the 11H and 12H $A_u$ HOOP vibration mode should be a major contributor to this doublet, and the 7H and 8H $A_u$ HOOP may also contribute. The relatively normal HOOP doublet frequency and intensity in Lumi suggest that the transition from bathorhodopsin to Lumi involves a relaxation of the chromophore to an unstrained all-trans conformation and the elimination of the structural perturbation that uncouples the 11H and 12H wags in bathorhodopsin. This conclusion is consistent with the previous studies of Lumi by CARS (*22*), low-temperature FTIR (*15*, *17*), and time-resolved UV−vis absorption (*13*, *41*) as well as NMR (*18*). Compared to that for Lumi, the major HOOP band in the Meta I spectrum appears at 957 $cm^{-1}$ and is assigned to an in-phase combination mode of the 11H and 12H wags. This peak is close to the frequency of the HOOP mode of the all-trans retinal PSB (*37*). Therefore, Meta I has a more normal all-trans retinal conformation, in line with previous Raman (*21*) and NMR results (*19*). This is further supported by the $^{13}C$ NMR chemical shift data, which probe the electronic structure of the chromophore in Meta I (*42*).

The respective ethylenic Raman frequencies of Lumi and Meta I show the expected linear correlation with the visual pigment absorption maxima (*27*), which in turn is a measure of the extent of charge delocalization in the electronic ground state. The ethylenic frequencies increase from 1533 $cm^{-1}$ in bathorhodopsin ($\lambda_{max}$ = 532 nm) to 1546 $cm^{-1}$ in rhodopsin ($\lambda_{max}$ = 498 nm), 1548 $cm^{-1}$ in Lumi ($\lambda_{max}$ = 492 nm), and 1551 $cm^{-1}$ in Meta I ($\lambda_{max}$ = 478 nm). This is consistent with the idea that the absorption maximum is correlated with the extent of charge delocalization in the chromophore ground state (*43*, *44*).

The protonated Schiff base C═N stretch frequency and its frequency shift in $D_2O$ provide important information about charge interactions and hydrogen bonding of the Schiff base group (*37*, *45*−*47*). The frequency shift of the C═N stretching band upon deuteration of the Schiff base nitrogen depends on the strength of its hydrogen bond with the environment, while the frequency of the C═ND stretching mode, which is primarily a function of electrostatic interactions between the Schiff base and its counterion, reports on the C═N bond order (*26*, *37*). The correlation between the deuteration shift and the hydrogen bonding strength results from the coupling of the C═N stretching mode with the N−H rocking mode. Deuteration of the nitrogen reduces this coupling as a result of the decreased N−D rocking frequency. A decreased level of hydrogen-bonding interaction with an environmental H-bond acceptor will lower the N−H rock frequency, causing a lower Schiff base stretch and a reduced deuteration-induced shift (*30*).

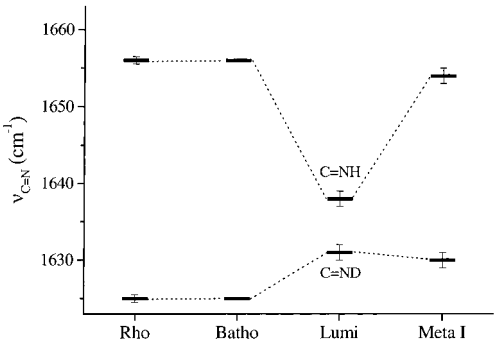


FIGURE 7: Frequencies of the C═NH and C═ND stretching modes of rhodopsin, bathorhodopsin, lumirhodopsin, and metarhodopsin I. The error bars indicate that the frequencies in our microchip experiments are accurate within ±1 $cm^{-1}$ for rhodopsin and ±2 $cm^{-1}$ for lumirhodopsin and metarhodopsin I.

As summarized in Table 1 and Figure 7, the C═N stretch frequencies of rhodopsin and bathorhodopsin are identical, and the ND shifts of ∼30 $cm^{-1}$ differ by only 5 $cm^{-1}$ (*8*), implying that the Schiff base group remains in nearly the same electrostatic and hydrogen-bonding environment immediately after cis−trans isomerization. Because rhodopsin and Lumi exhibit similar absorption maxima, the Schiff base vibrational properties might be expected to be similar (*26*). However, the C═N stretch in Lumi is observed at 1638 $cm^{-1}$, 18 $cm^{-1}$ below that of rhodopsin. The unusually low frequency of the C═N stretching mode in Lumi provides structural evidence that the interactions between the protein and the PSB group in Lumi are very different. Furthermore, the Schiff base stretching mode in Lumi shifts down by only 7 $cm^{-1}$ when Lumi is suspended in $D_2O$ buffer. This difference is predominantly due to the weaker coupling of the C═N stretch with the N−H bending vibration in Lumi. We conclude that the bathorhodopsin to Lumi process dramatically weakens the Schiff base hydrogen bonding. Our conclusion of weakened Schiff base hydrogen bonding in Lumi is in agreement with the FTIR studies (*15*).

In contrast, there is a significant frequency increase of the C═N stretching mode (from 1638 to 1654 $cm^{-1}$) in Meta I. The shift induced by deuteration (see Table 1) is also increased from ∼7 $cm^{-1}$ in Lumi to ∼24 $cm^{-1}$ in Meta I. The C═N frequency in Meta I and its shift in $D_2O$ buffer are identical to those of the all-trans PSB. This shows that the weakened Schiff base hydrogen bonding in Lumi recovers to the all-trans PSB value with the transition to Meta I (Figure

7). Also, the equivalence of the Schiff base stretching frequency of Lumi and Meta I in $D_2O$ argues that their C═N bond orders are similar. Thus, formation of the Meta I intermediate primarily involves a significant change in the hydrogen-bonding interaction between the Schiff base group and its protein environment. The Schiff base counterion in bovine rhodopsin is known to be Glu113 (*25*, *48*−*50*). Although the chromophore in bathorhodopsin is conformationally distorted, the Schiff base environment is similar to that in rhodopsin. Therefore, the protonated Schiff base counterion is likely to remain Glu113, together with one or more water molecules hydrogen bonded to Glu113, as evidenced by FTIR measurements (*51*). Because of the dramatic weakening of the Schiff base hydrogen bonding upon formation of Lumi from bathorhodopsin (Figure 7), it appears that there is essentially no H-bond acceptor in Lumi. This observation also implies that water is no longer hydrogen bonded to the PSB in Lumi. Thus, in Lumi the hydrogen-bonding environment is undergoing a transition from the native pocket in rhodopsin to a presumably more open solvent accessible environment in Meta I.

In summary, we have obtained high-quality transient Raman spectra of lumirhodopsin and metarhodopsin I using the new Raman microchip flow technique. When the Raman spectra of Lumi and Meta I are compared, the HOOP and fingerprint bands of the two intermediates are very similar. Thus, the chromophore appears to remain in a relaxed all-trans configuration and conformation in the transition from Lumi to Meta I. However, the protonated Schiff base C═N stretching modes of these two species are indicative of very different Schiff base environments. The transition from bathorhodopsin to Lumi thus involves chromophore relaxation and dramatic changes in the Schiff base region, while in the Lumi to Meta I transition, a fully relaxed chromophore with a normal Schiff base environment but a different hydrogen-bond acceptor is finally formed. Our experiments demonstrate that time-resolved resonance Raman spectroscopy using a Raman microprobe and the microchip flow technique provides a powerful and convenient tool for obtaining detailed structural information about microsecond to millisecond transient intermediates at room temperature. Our microchip flow technique could of course also be used to study photochemical kinetics. Future work will focus on the chromophore structure of the BSI intermediate to explore when the characteristic HOOP modes of bathorhodopsin disappear and when the unusual Schiff base environment in Lumi is formed.

## ACKNOWLEDGMENT

We thank Judy E. Kim, Michael J. Tauber, David McCamant, and Kevin Gaab for technical assistance and helpful discussions, Ziad Ganim for expert assistance with the rhodopsin preparations, and Charlie Emrich for making the microfabricated Raman flow chip.

## REFERENCES

1. Mathies, R. A., and Lugtenburg, J. (2000) in *Handbook of Biological Physics, Molecular Mechanism of Vision (Part 1)* (Stavenga, D. G., DeGrip, W. J., and Pugh, E. N., Jr., Eds.) pp 55−99, Elsevier Science Press, Amsterdam.
2. Schoenlein, R. W., Peteanu, L. A., Mathies, R. A., and Shank, C. V. (1991) *Science 254*, 412−415.
3. Kim, J. E., McCamant, D. W., Zhu, L., and Mathies, R. A. (2001) *J. Phys. Chem. B 105*, 1240−1249.
4. Kliger, D. S., and Lewis, J. W. (1995) *Isr. J. Chem. 35*, 289−307.
5. Stryer, L. (1986) *Annu. Rev. Neurosci. 9*, 87−119.
6. Peteanu, L. A., Schoenlein, R. W., Wang, Q., Mathies, R. A., and Shank, C. V. (1993) *Proc. Natl. Acad. Sci. U.S.A. 90*, 11762−11766.
7. Kandori, H., Shichida, Y., and Yoshizawa, T. (1989) *Biophys. J. 56*, 453−457.
8. Palings, I., Pardoen, J. A., van den Berg, E., Winkel, C., Lugtenburg, J., and Mathies, R. A. (1987) *Biochemistry 26*, 2544−2556.
9. Eyring, G., Curry, B., Broek, A., Lugtenburg, J., and Mathies, R. (1982) *Biochemistry 21*, 384−393.
10. Warshel, A., and Barboy, N. (1982) *J. Am. Chem. Soc. 104*, 1469−1476.
11. Birge, R. R. (1990) *Biochim. Biophys. Acta 1016*, 293−327.
12. Randall, C. E., Lewis, J. W., Hug, S. J., Bjorling, S., Eisner-Shanas, I., Friedman, N., Ottolenghi, M., Sheves, M., and Kliger, D. S. (1991) *J. Am. Chem. Soc. 113*, 3473−3485.
13. Hug, S. J., Lewis, J. W., Einterz, C. M., Thorgeirsson, T. E., and Kliger, D. S. (1990) *Biochemistry 29*, 1475−1485.
14. Thorgeirsson, T. E., Lewis, J. W., Wallace-Williams, S. E., and Kliger, D. S. (1992) *Photochem. Photobiol. 56*, 1135−1144.
15. Ganter, U. M., Gartner, W., and Siebert, F. (1988) *Biochemistry 27*, 7480−7488.
16. DeGrip, W. J., Gray, D., Gillespie, J., Bovee, P. H. M., van den Berg, E. M. M., Lugtenburg, J., and Rothschild, K. J. (1988) *Photochem. Photobiol. 48*, 497−504.
17. Ohkita, Y. J., Sasaki, J., Maeda, A., Yoshizawa, T., Groesbeek, M., Verdegem, P., and Lugtenburg, J. (1995) *Biophys. Chem. 56*, 71−78.
18. Verdegem, P. J. E. (1998) Ph.D. Thesis, pp 1−299, Leiden Institute of Chemistry, Leiden Univeristy, Leiden, The Netherlands.
19. Verdegem, P. J. E., Bovee-Geurts, P. H. M., de Grip, W. J., Lugtenburg, J., and de Groot, H. J. M. (1999) *Biochemistry 38*, 11316−11324.
20. Lewis, J. W., Einterz, C. M., Hug, S. J., and Kliger, D. S. (1989) *Biophys. J. 56*, 1101−1111.
21. Doukas, A. G., Aton, B., Callender, R. H., and Ebrey, T. G. (1978) *Biochemistry 17*, 2430−2435.
22. Ujj, L., Jager, F., and Atkinson, G. H. (1998) *Biophys. J. 74*, 1492−1501.
23. Barry, B., and Mathies, R. A. (1982) *J. Cell Biol. 94*, 479−482.
24. Loppnow, G. R., Barry, B. A., and Mathies, R. A. (1989) *Proc. Natl. Acad. Sci. U.S.A. 86*, 1515−1518.
25. Lin, S. W., Sakmar, T. P., Franke, R. R., Khorana, H. G., and Mathies, R. A. (1992) *Biochemistry 31*, 5105−5111.
26. Lin, S. W., Imamoto, Y., Fukada, Y., Shichida, Y., Yoshizawa, T., and Mathies, R. A. (1994) *Biochemistry 33*, 2151−2160.
27. Kochendoerfer, G. G., Wang, Z., Oprian, D. D., and Mathies, R. A. (1997) *Biochemistry 36*, 6577−6587.
28. Kochendoerfer, G. G., Lin, S. W., Sakmar, T. P., and Mathies, R. A. (1999) *Trends Biochem. Sci. 24*, 300−305.
29. Mathies, R. A., Oseroff, A. R., and Stryer, L. (1976) *Proc. Natl. Acad. Sci. U.S.A. 73*, 1−5.
30. Mathies, R. A., Smith, S. O., and Palings, I. (1987) in *Biological Applications of Raman Spectroscopy: Resonance Raman Spectra of Polyenes and Aromatics* (Spiro, T. G., Ed.) pp 59−108, John Wiley and Sons, New York.
31. Simpson, P. C., Woolley, A. T., and Mathies, R. A. (1998) *J. Biomed. Microdevices 1*, 7−26.
32. Shi, Y., Simpson, P. C., Scherer, J. R., Wexler, D., Skibola, C., Smith, M. T., and Mathies, R. A. (1999) *Anal. Chem. 71*, 5354−5361.
33. Lagally, E. T., Medintz, I., and Mathies, R. A. (2001) *Anal. Chem. 73*, 565−570.

34. Applebury, M. L., Zuckerman, D. M., Lamola, A. A., and Jovin, T. M. (1974) *Biochemistry 13*, 3448−3458.
35. Mathies, R., and Yu, N.-T. (1978) *J. Raman Spectrosc. 7*, 349−352.
36. Lin, S. W., Groesbeek, M., van der Hoef, I., Verdegem, P., Lugtenburg, J., and Mathies, R. A. (1998) *J. Phys. Chem. B 102*, 2787−2806.
37. Smith, S. O., Myers, A. B., Mathies, R. A., Pardoen, J. A., Winkel, C., van den Berg, E. M. M., and Lugtenburg, J. (1985) *Biophys. J. 47*, 653−664.
38. Curry, B., Broek, A., Lugtenburg, J., and Mathies, R. (1982) *J. Am. Chem. Soc. 104*, 5274−5286.
39. Siebert, F. (1995) *Isr. J. Chem. 35*, 309−323.
40. Horiuchi, S., Tokunaga, F., and Yoshizawa, T. (1980) *Biochim. Biophys. Acta 591*, 445−447.
41. Nakagawa, M., Kikkawa, S., Iwasa, T., and Tsuda, M. (1997) *Biophys. J. 72*, 2320−2328.
42. Harbison, G. S., Smith, S. O., Pardoen, J. A., Courtin, J. M. L., Lugtenburg, J., Herzfeld, J., Mathies, R. A., and Griffin, R. G. (1985) *Biochemistry 24*, 6955−6962.
43. Aton, B., Doukas, A. G., Callender, R. H., Becher, B., and Ebrey, T. G. (1977) *Biochemistry 16*, 2995−2999.
44. Albeck, A., Livnah, N., Gottlieb, H., and Sheves, M. (1992) *J. Am. Chem. Soc. 114*, 2400−2411.
45. Baasov, T., Friedman, N., and Sheves, M. (1987) *Biochemistry 26*, 3210−3217.
46. Kakitani, H., Kakitani, T., Rodman, H., and Honig, B. (1985) *Photochem. Photobiol. 41*, 471−479.
47. Rodman-Gilson, H. S., Honig, B. H., Croteau, A., Zarrilli, G., and Nakanishi, K. (1988) *Biophys. J. 53*, 261−269.
48. Nathans, J. (1990) *Biochemistry 29*, 937−942.
49. Sakmar, T. P., Franke, R. R., and Khorana, H. G. (1989) *Proc. Natl. Acad. Sci. U.S.A. 86*, 8309−8313.
50. Zhukovsky, E. A., and Oprian, D. D. (1989) *Science 246*, 928−930.
51. Nagata, T., Terakita, A., Kandori, H., Shichida, Y., and Maeda, A. (1997) *Biochemistry 36*, 6164−6170.

BI010670X